# Mechanistic basis for receptor-mediated pathological α-synuclein fibril cell-to-cell transmission in Parkinson's disease

Shengnan Zhang[a,1], Yu-Qing Liu[b,1], Chunyu Jia[a,c,1], Yeh-Jun Lim[b,1], Guoqin Feng[d,e,1], Enquan Xu[f,g], Houfang Long[a,c], Yasuyoshi Kimura[f,g], Youqi Tao[h], Chunyu Zhao[a,c], Chuchu Wang[a,c], Zhenying Liu[a,c], Jin-Jian Hu[b], Meng-Rong Ma[b], Zhijun Liu[i], Lin Jiang[j], Dan Li[h], Renxiao Wang[d,e,k], Valina L. Dawson[f,g,l,m,n], Ted M. Dawson[f,g,l,n,o,2], Yan-Mei Li[b,2], Xiaobo Mao[f,g,2], and Cong Liu[a,2]

[a]Interdisciplinary Research Center on Biology and Chemistry, Shanghai Institute of Organic Chemistry, Chinese Academy of Sciences, Shanghai 201210, China; [b]Key Laboratory of Bioorganic Phosphorus Chemistry & Chemical Biology (Ministry of Education), Department of Chemistry, Tsinghua University, Beijing 100084, China; [c]University of Chinese Academy of Sciences, Beijing 100049, China; [d]State Key Laboratory of Bio-organic Chemistry and Natural Products Chemistry, Center for Excellence in Molecular Synthesis, Shanghai Institute of Organic Chemistry, Chinese Academy of Sciences, Shanghai 200032, China; [e]Department of Medicinal Chemistry, School of Pharmacy, Fudan University, Shanghai 201203, China; [f]Neuroregeneration and Stem Cell Programs, Institute for Cell Engineering, Johns Hopkins University School of Medicine, Baltimore, MD 21205; [g]Department of Neurology, Johns Hopkins University School of Medicine, Baltimore, MD 21205; [h]Key Laboratory for the Genetics of Developmental and Neuropsychiatric Disorders (Ministry of Education), Bio-X Institutes, Shanghai Jiao Tong University, Shanghai 200030, China; [i]National Center for Protein Science Shanghai, Zhangjiang Lab, Shanghai Advanced Research Institute, Chinese Academy of Sciences, Shanghai 201210, China; [j]Department of Neurology, David Geffen School of Medicine, University of California Los Angeles, CA 90095; [k]Shanxi Key Laboratory of Innovative Drugs for the Treatment of Serious Diseases Based on Chronic Inflammation, College of Traditional Chinese Medicines, Shanxi University of Chinese Medicine, Taiyuan, Shanxi 030619, China; [l]Adrienne Helis Malvin Medical Research Foundation, New Orleans, LA 70130; [m]Department of Physiology, Johns Hopkins University School of Medicine, Baltimore, MD 21205; [n]Solomon H. Snyder Department of Neuroscience, Johns Hopkins University School of Medicine, Baltimore, MD 21205; and [o]Department of Pharmacology and Molecular Sciences, Johns Hopkins University School of Medicine, Baltimore, MD 21205

Edited by Robert Tycko, National Institute of Diabetes and Digestive and Kidney Diseases, Bethesda, MD, and approved May 24, 2021 (received for review June 2, 2020)

**The spread of pathological α-synuclein (α-syn) is a crucial event in the progression of Parkinson's disease (PD). Cell surface receptors such as lymphocyte activation gene 3 (LAG3) and amyloid precursor-like protein 1 (APLP1) can preferentially bind α-syn in the amyloid over monomeric state to initiate cell-to-cell transmission. However, the molecular mechanism underlying this selective binding is unknown. Here, we perform an array of biophysical experiments and reveal that LAG3 D1 and APLP1 E1 domains commonly use an alkaline surface to bind the acidic C terminus, especially residues 118 to 140, of α-syn. The formation of amyloid fibrils not only can disrupt the intramolecular interactions between the C terminus and the amyloid-forming core of α-syn but can also condense the C terminus on fibril surface, which remarkably increase the binding affinity of α-syn to the receptors. Based on this mechanism, we find that phosphorylation at serine 129 (pS129), a hallmark modification of pathological α-syn, can further enhance the interaction between α-syn fibrils and the receptors. This finding is further confirmed by the higher efficiency of pS129 fibrils in cellular internalization, seeding, and inducing PD-like α-syn pathology in transgenic mice. Our work illuminates the mechanistic understanding on the spread of pathological α-syn and provides structural information for therapeutic targeting on the interaction of α-syn fibrils and receptors as a potential treatment for PD.**

α-synuclein | Parkinson's disease | cell-to-cell transmission | posttranslational modification

Aggregation and the spread of amyloid proteins, such as α-synuclein (α-syn), amyloid-β, Tau, and TDP43, are critical events in the pathogenesis of neurodegenerative disorders, including Parkinson's disease (PD), Alzheimer's disease, and amyotrophic lateral sclerosis, respectively (1, 2). As the hallmark of PD and other α-synucleinopathies, α-syn aggregation spreads in a prion-like progressive and stepwise manner both within the brain and from other organs to the brain during disease progression (3–7). Pathological α-syn aggregation can template monomeric α-syn to aggregate and participate in disease pathogenesis. Pathological α-syn inclusion can spread in the grafted neurons of PD patients (4, 8). Brain extracts from patients with multiple system atrophy can transmit neurodegeneration to genetically engineered mice (9). A single administration of α-syn preformed fibrils (PFFs) in mouse brains can recapitulate the pathological phenotypes of α-synucleinopathies (10–13).

Selected cell surface proteins, such as lymphocyte activation gene 3 (LAG3) and amyloid precursor-like protein 1 (APLP1), have been found to serve as receptors for α-syn PFF internalization and transmission (10, 14, 15). Intriguingly, these receptors preferentially recognize α-syn PFFs rather than the monomer (10). The α-syn monomer is intrinsically disordered and forms α-helical conformation upon membrane binding as involved in synaptic vesicle

## Significance

Receptor-mediated cell-to-cell transmission of pathological α-synuclein (α-syn) plays an important role in the progression of Parkinson's disease (PD). We show that α-syn uses its acidic C terminus to bind an alkaline patch on the receptors. The formation of amyloid fibrils dramatically enhances the binding by condensing α-syn molecules and better exposing the C terminus. Moreover, S129 phosphorylation, a hallmark modification of α-syn accumulation in Lewy bodies, further strengthens the electrostatic interactions between α-syn and the receptors, which accelerates the PD-like pathology in mice. This work illuminates mechanistic understanding on the spread of pathological proteins and provides structural information for the therapeutic targeting of pathological α-syn spread in PD progression.

Author contributions: S.Z., D.L., R.W., V.L.D., T.M.D., Y.-M.L., X.M., and C.L. designed research; S.Z., Y.-Q.L., C.J., Y.-J.L., G.F., E.X., H.L., Y.K., Y.T., C.Z., C.W., Zhenying Liu, J.-J.H., M.-R.M., and L.J. performed research; S.Z., Y.-Q.L., C.J., Y.-J.L., G.F., E.X., H.L., Y.K., Y.T., Zhijun Liu, L.J., and R.W. analyzed data; and S.Z., D.L., T.M.D., Y.-M.L., X.M., and C.L. wrote the paper.

The authors declare no competing interest.

This article is a PNAS Direct Submission.



[1]S.Z., Y.-Q.L., C.J., Y.-J.L., and G.F. contributed equally to this work.

[2]To whom correspondence may be addressed. Email: tdawson@jhmi.edu, liym@mail.tsinghua.edu.cn, xmao4@jhmi.edu, or liulab@sioc.ac.cn.

This article contains supporting information online at https://www.pnas.org/lookup/suppl/doi:10.1073/pnas.2011196118/-/DCSupplemental.

Published June 25, 2021.

trafficking (16–19). Cryogenic electron microscopic (cryo-EM) structures of full-length α-syn amyloid fibrils show that the central region of α-syn, approximately covering residues 37 to 99, is involved in the formation of a cross-β fibril core (termed as FC region), while the remaining *N* and C termini remain flexible (20–24). Despite the recent successes in the structural determination of α-syn amyloid fibrils, considerable challenges remain in linking the structural information to α-syn pathology. The structural basis underlying α-syn transmission, specifically the interplay between α-syn PFFs and receptors, is unknown. It also remains unclear how receptors, for example, LAG3 and APLP1, selectively recognize α-syn PFFs over monomers, nor do we know the role of posttranslational modification of α-syn in this process.

In this work, we combined multiple biophysical, cellular, and in vivo approaches to reveal the structural basis underlying the receptor binding of α-syn amyloid fibrils during cell-to-cell transmission. We found that the D1 domain of LAG3 utilizes a positively charged surface to capture the acidic C terminus of

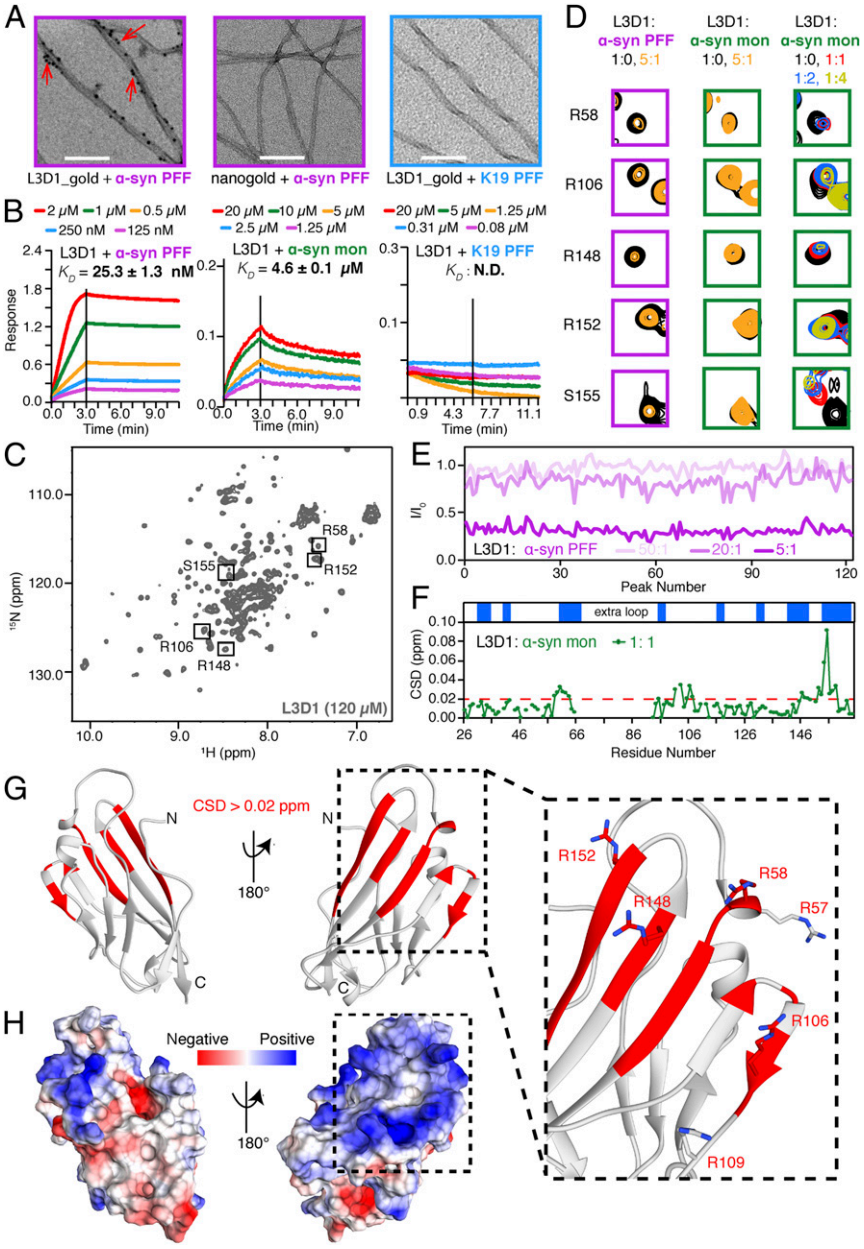


**Fig. 1.** L3D1 uses a positively charged surface to bind with α-syn. (*A*) TEM images of PFFs of α-syn and Tau K19 incubated with His-tagged L3D1 and probed by nanogolds. Red arrows indicate the attachment of nanogolds on PFFs. (Scale bar, 200 nm.) (*B*) Kinetic binding curves of L3D1 with α-syn PFFs (*Left*), α-syn monomers (*Middle*), and K19 PFFs (*Right*) by BLI. The association and dissociation profiles are divided by a vertical black line. N.D., not detectable. (*C*) The 2D $^{1}$H-$^{15}$N HSQC spectrum of L3D1 in 50 mM sodium phosphate and 50 mM NaCl, pH 7.0. The resonances that are enlarged in *D* are boxed and labeled. (*D*) Representative resonances from the HSQC spectra of L3D1 titrated by α-syn PFFs (magenta boxes) and monomers (green boxes). Molar ratios are indicated. (*E*) Intensity changes of L3D1 resonances titrated by α-syn PFFs at three different molar ratios. (*F*) Residue-specific CSDs of L3D1 in the presence of α-syn monomers. (*Top*) The secondary structure of L3D1 with blue boxes representing β-strands. The red dashed line indicates the CSDs of 0.02 ppm. (*G*) The structural model of dL3D1 is shown in cartoon. The residues with CSDs > 0.02 ppm in *F* are highlighted in red. (*Right*) Key interacting residues R57, R58, R106, R109, R148, and R152 are shown in a zoomed-in view. (*H*) Electrostatic surface of dL3D1. The structure is shown in the same view, and the same region is framed as in *G*.

α-syn, which is exposed and concentrated on the surface of α-syn fibrils. In contrast, α-syn monomers adopt a self-shielded conformation to impede the exposure of the C terminus. Phosphorylation at serine 129 (pS129) of α-syn, a pathological biomarker in PD (25–27), significantly enhances the binding of α-syn PFFs to LAG3 and APLP1 and promotes the cell-to-cell transmission in vitro and in vivo. Our work provides the structural basis for the receptor-mediated neuronal internalization and transmission of α-syn fibrils and suggests that the C terminus, specifically residues 118 to 140, is a pathological epitope of α-syn for receptor binding and thus may serve as a promising target for the therapeutic drug development to block PD progression.

## Results

**LAG3 D1 Preferably Binds α-Syn PFFs with a High Affinity.** The LAG3 D1 domain (L3D1) is essential for the internalization of α-syn PFFs (10). To determine the direct interaction between LAG3 and α-syn PFFs, we first incubated purified recombinant His-tagged L3D1 with α-syn PFFs. The direct binding of L3D1 to α-syn PFFs was visualized by negative-staining transmission electron microscopy (TEM). Using nanogold particles, which can bind with the His-tag, we observed that L3D1 carpeted the surface of α-syn PFFs (Fig. 1*A*). As a negative control, in the absence of L3D1, few nanogold particles attached to α-syn PFFs (Fig. 1*A*). Since amyloid fibrils formed by different proteins share a common cross-β structure, to rule out the possibility that L3D1 generally binds the cross-β structure, we used Tau K19 as another control. Similar to α-syn, K19 is intrinsically disordered and aggregates into amyloid fibrils with similar twisted morphology under TEM. However, no binding was observed between K19 PFFs and L3D1 suggesting the specificity of L3D1 binding to α-syn PFFs (Fig. 1*A*).

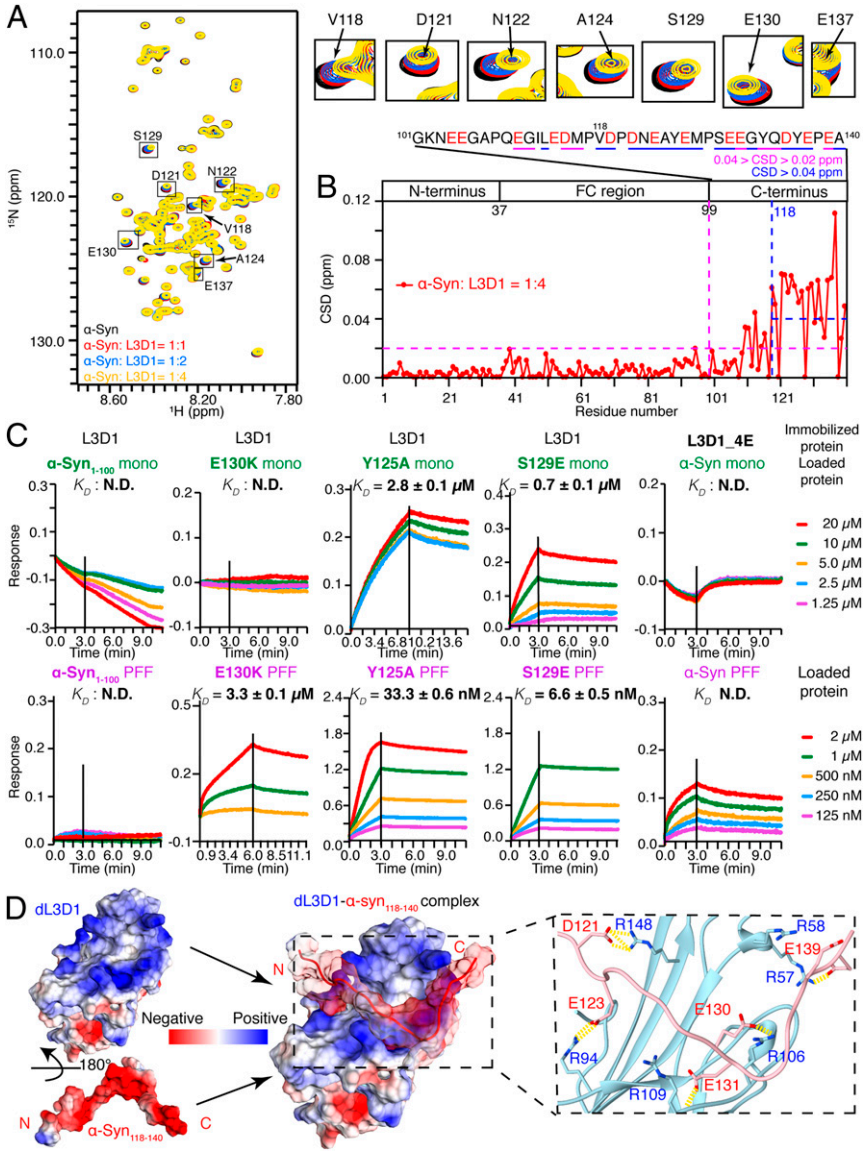


**Fig. 2.** α-Syn uses its C terminus to bind with L3D1. (*A*) Overlay of the 2D $^{1}H$-$^{15}N$ HSQC spectra of 25 μM α-syn alone (black) and in the presence of L3D1 at molar ratios of 1:1 (red), 1:2 (blue), and 1:4 (yellow), respectively. (*Right*) Representative residues with significant CSDs zoomed in. (*B*) Calculated CSDs of α-syn in the presence of L3D1 at the molar ratio of 1:4. The domain organization of α-syn is shown. The blue and magenta dashed lines indicate the residues with CSDs > 0.04 and 0.02 ppm, respectively, which are also underscored in the primary sequence shown (*Top*). The acidic residues in the C terminus are highlighted in red. (*C*) BLI-binding kinetics of L3D1 with α-syn variants in the forms of monomer (*Upper*) and PFFs (*Lower*), respectively. N.D., not detectable. (*D*) Electrostatic surface of the representative complex structure of dL3D1–α-syn$_{118–140}$, which is built by HADDOCK. (*Right*) The complex interface zoomed in.

We next used bio-layer interferometry (BLI) assay to measure the binding affinity between L3D1 and α-syn. L3D1 was immobilized on the biosensor and incubated with varying concentrations of α-syn PFFs or monomers in solution. The result showed that the equilibrium dissociation constant ($K_D$) of L3D1 to α-syn PFFs was 25.3 ± 1.3 nM, which was ~200-fold higher than that of L3D1 to α-syn monomer (4.6 ± 0.1 μM) (Fig. 1*B*). The N-terminal His-tag of L3D1 showed neglectable influence on the binding (*SI Appendix*, Fig. S1*A*). To cross-validate the measurement, we fixed α-syn PFFs on the biosensor and incubated with varying concentrations of L3D1. The result showed a consistent $K_D$ of 33.3 ± 9.2 nM (*SI Appendix*, Fig. S1*B*). In addition, we used surface plasmon resonance assay to confirm the BLI measurement and obtained a similar binding affinity of α-syn PFFs to L3D1 (*SI Appendix*, Fig. S1*C*). Again, Tau K19 PFFs as a negative control showed no appreciable binding to L3D1 (Fig. 1*B*). These results demonstrate that L3D1 directly binds to α-syn with a markedly higher affinity to the fibrillar form than to the monomeric form of α-syn, which is consistent with our previous observation at the cellular level (10).

**L3D1 Utilizes a Positively Charged Surface to Bind with α-Syn.** To probe the binding surface of L3D1 to α-syn, we performed solution NMR spectroscopy. The two-dimensional (2D) $^{1}H$-$^{15}N$ heteronuclear single-quantum coherence (HSQC) spectrum of $^{15}N$-labeled L3D1 was well dispersed with nearly 120 discrete signals, indicative of a well-folded structure (Fig. 1*C*). However, the clustering of signals with high intensity in the random coil region (8.6 to 7.8 ppm) suggests that a portion of L3D1 is intrinsically disordered. And the high intensity of these random coil residues makes it difficult to assign the well-folded residues with weaker intensities. To solve this technical difficulty, we first built a structural model of L3D1 by Rosetta modeling. The structure features a typical Ig fold consisting of two antiparallel β sheets and an extra loop (*SI Appendix*, Fig. S2). The extra loop was previously identified as essential in mediating LAG3 binding to major histocompatibility complex class II (MHC-II) (28). Intriguingly, we found that truncation of this extra loop does not impair the binding of L3D1 to either α-syn PFFs or monomers (*SI Appendix*, Fig. S3*A*). In addition, truncation of the extra loop eliminated the high intensity signals in the random coil region of the spectrum but left the more dispersed lower intensity signals unperturbed (*SI Appendix*, Fig. S4*A*), indicating that the extra loop is not necessary for the proper folding of L3D1. We achieved the backbone assignments of the truncated L3D1 (dL3D1) using three-dimensional (3D) NMR (*SI Appendix*, Fig. S4*B*) and mapped the residues involved in β strands determined by the NMR assignments on the structural model of L3D1. They matched well with the computational structure, providing validation for the structural prediction of L3D1 (*SI Appendix*, Fig. S4*C*).

Next, we titrated L3D1 with α-syn. The titration of substoichiometric α-syn PFFs led to a global HSQC intensity drop of L3D1 in a concentration-dependent manner (Fig. 1 *D* and *E* and *SI Appendix*, Fig. S5*A*), which reflects a substantial increase of molecular weight upon the binding of α-syn PFFs to L3D1. In contrast, no appreciable change was detected by the titration of the α-syn monomer at the substoichiometric ratio (*SI Appendix*, Fig. S5 *B* and *C*). Next, we increased the α-syn concentration and titrated excess α-syn monomers to L3D1. The HSQC spectra showed significant chemical shift deviations (CSDs) (Fig. 1 *D* and *F* and *SI Appendix*, Fig. S5*D*). By mapping the residues with CSDs > 0.02 ppm on a dL3D1 structure model, we found that these residues clustered on one of the β sheets (Fig. 1*G*) where the surface was markedly positively charged (Fig. 1*H*). To confirm the role of electrostatic interactions in the recognition of α-syn by the receptor, we tested the binding of α-syn to L3D1 in the presence of 500 mM or 1 M salt. The result showed that high salt concentrations disrupted the binding with no detectable association between α-syn and L3D1 by BLI (*SI Appendix*, Fig. S3 *B* and *C*). These results suggest that electrostatic interaction plays a key role in mediating L3D1–α-syn interaction.

**α-Syn Uses Its Acidic C Terminus to Bind with L3D1.** We next sought to identify the region of α-syn involved in the binding with L3D1. The titration of L3D1 to the $^{15}N$-labeled α-syn monomer resulted in significant CSDs of the residues mostly in the C terminus (CSDs > 0.02 ppm), especially residues 118 to 140 (CSDs > 0.04 ppm) (Fig. 2 *A* and *B*). The deletion of the C terminus (the construct is referred to as α-syn$_{1–100}$) completely abolished the binding of L3D1 with both the α-syn monomer and PFFs measured by BLI (Fig. 2*C*, column one) and NMR experiments (*SI Appendix*, Fig. S6). Conversely, the removal of residues 1 to 100 (the resulting construct is referred to as α-syn$_{101–140}$) showed no marked influence on L3D1 binding measured by BLI (*SI Appendix*, Fig. S3*D*). To further assess the importance of the C terminus in binding with L3D1, we conjugated the C terminus (α-syn$_{101–140}$) to Tau K19, which does not bind with L3D1 (Fig. 1 *A* and *B*). Remarkably, the fusion the of α-syn C terminus to K19 (the construct is referred to K19–α-syn$_{101–140}$) resulted in the strong binding of K19 PFFs to L3D1 with a similar affinity to that of the α-syn PFF-L3D1 binding (*SI Appendix*, Fig. S3*E*). α-Syn PFFs alone were digested significantly faster by Proteinase K (PK) than that incubated with L3D1 (*SI Appendix*, Fig. S7), indicating that the protease sensitive C terminus of α-syn PFFs is resistant to digestion in the presence of L3D1. Altogether, these results suggest that the C terminus of α-syn plays a key role in L3D1 binding.

To further characterize the L3D1–α-syn interaction, we modeled the structure of dL3D1 in complex with α-syn$_{118–140}$ by HADDOCK (*SI Appendix*, Fig. S8 and Table S1) (29) according to the NMR and BLI data. The energy profile and stability of the docked complex models of dL3D1–α-syn$_{118–140}$ were further assessed by molecular dynamics (MD) simulation and molecular mechanics generalized Born and surface area (MM-GBSA) analysis. The most dominant structure (~59%) among the 8,000 simulated conformations is shown in Fig. 2*D* in which the acidic α-syn C terminus is well accommodated on the alkaline surface of dL3D1. The complex structure showed that five alkaline residues from L3D1 (R57, R94, R106, R109, and R148) and five acidic residues from α-syn (D121, E123, E130, E131, and E139) are on the interface of the complex (Fig. 2*D*). Residue-based free energy decomposition analysis by MM-GBSA identified four alkaline residues of dL3D1 including R57, R58, R106, and R109, which are important for stabilizing the complex structure (*SI Appendix*, Fig. S8*D*). These computational data provide additional support to demonstrate the important role of the electrostatic interaction in the binding of α-syn with L3D1.

We next performed a mutagenesis study to experimentally validate the complex structure of α-syn and L3D1 obtained from NMR and the modeling study. Notably, the mutation of α-syn E130 to Lys (K) severely impaired the binding of both the α-syn monomer and PFFs with L3D1 (Fig. 2*C*, column two and *SI Appendix*, Fig. S6 *C* and *D*) by both BLI and NMR experiments. While the mutation of Y125, which is not on the interface (*SI Appendix*, Fig. S9*A*), to Ala (A) did not significantly influence the binding (Fig. 2*C*, column three). Intriguingly, we found that the S129E mutation, which mimics the phosphorylated S129, dramatically increased the binding affinity between α-syn and L3D1 by one order of magnitude (Fig. 2*C*, column four and *SI Appendix*, Fig. S9*B*). We confirmed that the above mutations did not change the morphology of α-syn amyloid fibrils by TEM (*SI Appendix*, Fig. S10*A*), nor did they change the PFF length by atomic-force microscopy (AFM) (*SI Appendix*, Fig. S10*B*), which is consistent with their location being outside of the FC region. In addition, mutations of four key arginine residues of L3D1, including R57, R58, R106, and R109, to negatively charged E (L3D1_4E) massively weakened the interaction between α-syn and L3D1 (Fig. 2*C*, column five and

*SI Appendix*, Figs. S9*C* and S11 *A* and *B*) without impairing the overall configuration of L3D1 (*SI Appendix*, Fig. S11*C*). Altogether, our data provides the structural basis of the interaction between the acidic C terminus of α-syn and L3D1.

**The C Terminus Is Shielded in α-Syn Monomer but Exposed and Condensed on Fibril.** Next, we sought to ask why L3D1 preferentially binds with α-syn fibrils over the monomer. Although α-syn presents as an intrinsically disordered monomer in solution and in cells, previous studies showed that its C terminus forms transient long-range interactions with the central region, which may inhibit α-syn aggregation (16, 30–32). Thus, we wondered whether the conformation of the α-syn monomer might hinder its binding with L3D1. To test this hypothesis, we first probed the transient and long-range interactions (<24 Å) within and between α-syn monomers by paramagnetic relaxation enhancement (PRE) NMR using a nitroxide spin label—S-(1-oxyl-2,2,5,5-tetramethyl-2,5-dihydro-1H-pyrrol-3-yl) methyl methanesulfonothioate (MTSL) (Fig. 3*A*). We introduced MTSL at A124 of the $^{15}$N-labeled α-syn monomer to monitor its potential long-range contacts by measuring the intensity ratio ($I_{param}/I_{diam}$) of each residue (Fig. 3*B*). The result showed that residues 117 to 129 experienced local PRE effects with the line broadening beyond the detection limit because of their adjacent positions to the label site (Fig. 3*B*). Notably, residues 34 to 43 and 89 to 101 that are at both ends of the FC region encountered significant intensity drops despite a slight global intensity drop under our experimental condition (Fig. 3*B*). Consistent with our observation, similar PRE interaction of the C-terminal region with residues 36 to 42 has been reported recently (32). To further validate, we conversely labeled E35 with MTSL and indeed observed significant intensity drops around residues 115 to 133 (Fig. 3*C*). Thus, these data indicate that residues 34 to 43 and 89 to 101 may spatially get close to the C terminus.

To further investigate whether the interactions are intra- or intermolecular, we mixed $^{15}$N-labeled α-syn with α-syn that was MTSL labeled but not $^{15}$N labeled (NMR invisible) (Fig. 3*A*). By this means, only intermolecular interactions can be detected. The result showed no significant intensity change of $^{15}$N-labeled α-syn (Fig. 3 *B* and *C*, gray lines), indicating that the interactions between the C terminus and FC region are intramolecular. Long-range intramolecular interactions of α-syn have also been observed by other groups using PRE experiments with MTSL labeled at different residues of α-syn (16, 30–32). Thus, in line with previous studies, our results highlight that the α-syn monomer adopts a dynamic self-shielded structure with long-range and transient interactions between the C terminus and the termini of the FC region.

To test the influence of these intramolecular interactions on the binding of α-syn to L3D1, we deleted residues 34 to 43 of α-syn (the resulting construct is referred to as α-syn$_{\Delta(34\text{-}43)}$) to weaken the interaction of this region with the C terminus. Indeed, the

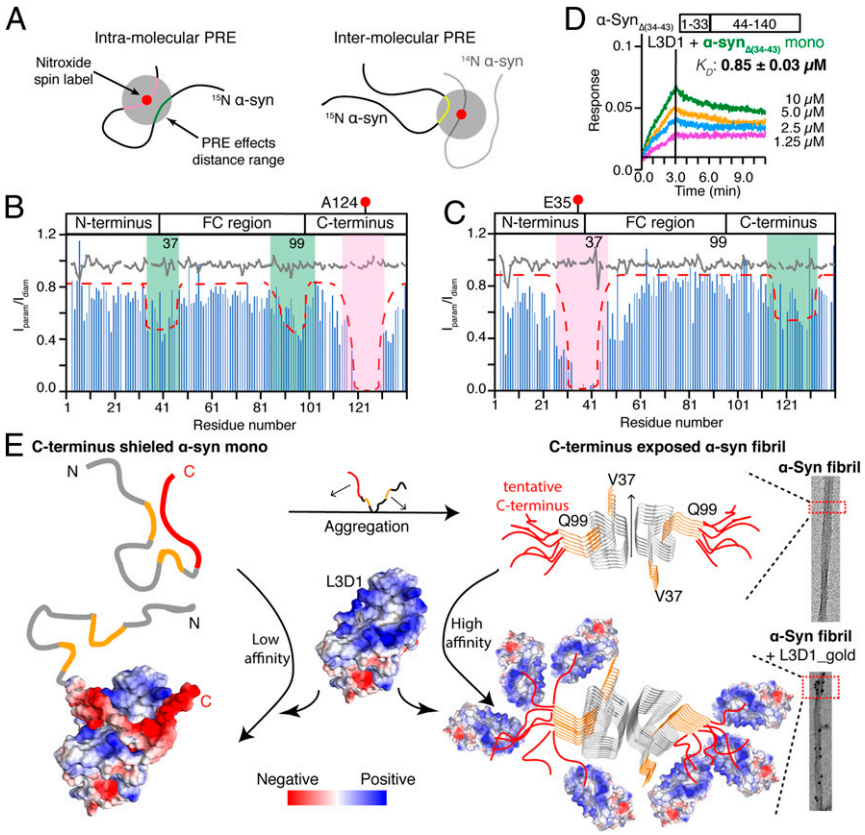


**Fig. 3.** Mechanism of the preferential binding of L3D1 with α-syn fibrils over the monomer. (*A*) Schematic diagram of the NMR PRE for probing the intra- and intermolecular long-range interactions in α-syn monomers. The adjacent residues (pink) and the residues in spatial contacts (light green and yellow) with the nitroxide spin label exhibit the PRE effects. (*B* and *C*) PRE profiles of $^{15}$N-labeled MTSL-A124C-α-syn (*B*) and MTSL-E35C-α-syn (*C*). The paramagnetic effects are highlighted by dashed lines and pink/green shades. The gray lines stand for the result of intermolecular PRE experiments in which $^{15}$N-α-syn was incubated with NMR inactive ($^{14}$N) MTSL-A124C-α-syn (*B*) or MTSL-E35C-α-syn (*C*). (*D*) BLI-binding kinetics of L3D1 with the α-syn$_{\Delta(34\text{-}43)}$ monomer. (*E*) Schematic illustration of the structural mechanism by which L3D1 preferentially binds with α-syn fibrils over the monomer. The α-syn monomer adopts a self-shielded conformation with transient contacts between the C terminus (red) and both ends of the FC region (orange), which inhibits L3D1 binding. As forming amyloid fibrils, α-syn exposes and condenses the C termini, which significantly enhance the binding with L3D1. The flexible C termini are tentatively drawn on the cryo-EM fibril structure of α-syn (Protein Data Bank identification: 6A6B).

results showed that the deletion of this region significantly increased the binding affinity of the α-syn monomer to L3D1 from 4.6 ± 0.1 to 0.85 ± 0.03 μM (Fig. 3*D*). While this deletion impairs the amyloid fibril formation of α-syn (*SI Appendix*, Fig. S10*C*), which has been shown previously with a similar deletion variant (32). Altogether, these results demonstrate that the intramolecular interactions shield the C terminus from L3D1 binding. In contrast, when α-syn forms amyloid fibrils, the FC region is involved in the formation of the fibril spine, and thus, the C terminus is released and available for the L3D1 binding (Fig. 3*E*). Moreover, in the fibrillar form, the alignment of C termini along the fibril axis largely increases its local concentration. AFM measurements showed that our PFF samples contain fibrils mainly with a length of ∼50 nm (*SI Appendix*, Fig. S10*B*). Given that there are two α-syn molecules in one layer of the fibril and the distance between layers is 4.8 Å (20), we may calculate that there are roughly 200 α-syn molecules in a single PFF, that is, α-syn is ∼200 times concentrated in PFFs. While it is worthwhile to note that the mobility of α-syn molecules in fibrils is limited to some extent, fibril formation and C-terminal exposure are synergistic conformational changes of α-syn. Therefore, these results suggest that the structural rearrangement and condensation of the C terminus in fibrils together determine the remarkably enhanced binding affinities to L3D1.

**Phosphorylation at S129 Enhances the Binding of α-Syn Fibril to LAG3.** pS129 α-syn is a pathological hallmark for Lewy bodies and Lewy neurites widely found in the brains of PD patients and α-synucleinopathies (25–27). We have shown that S129E, a pS129 mimicking mutation, increases the binding of α-syn with L3D1 (Fig. 2*C*, column four). To further assess the role of S129 phosphorylation, we semisynthesized pS129 α-syn (*SI Appendix*, Fig. S12) (33, 34). pS129 α-syn formed amyloid fibrils with similar morphology to that of the nonphosphorylated wild-type (WT) α-syn (35) (Fig. 4*A* and *SI Appendix*, Fig. S10). Remarkably, the pS129 PFFs exhibited a significantly increased binding affinity to L3D1 with a $K_D$ value of 1.4 ± 1.6 nM (Fig. 4*B*) compared to 25.3 ± 1.3 nM of the WT α-syn PFFs (Fig. 1*B*). The pS129 α-syn monomer also exhibited an enhanced binding affinity of 0.37 ± 0.01 μM in comparison with 4.6 ± 0.1 μM of the WT (Fig. 4*B*).

To gain the structural insight of the enhanced binding by S129 phosphorylation, we performed computational modeling and MD simulation to characterize the interaction of pS129 α-syn$_{118–140}$ and dL3D1 (*SI Appendix*, Table S1). The structure model showed that S129 phosphorylation did not change the overall structure of the complex, while the phosphate group of pS129 was directly involved in the complex interface (Fig. 4*C*), which resulted in a significantly lower free binding energy of −87.96 kcal/mol compared to that of the nonphosphorylated complex (−76.36 kcal/mol) (*SI Appendix*, Table S2).

We further determined whether pS129 increased the binding of α-syn PFFs to human full-length LAG3 in cells. The PFFs of human WT, pS129, and α-syn$_{1–100}$ were prepared and biotinylated, which were characterized by immunoblot analysis, TEM, and AFM (*SI Appendix*, Figs. S10 and S13). These results suggest that the WT, pS129, and α-syn$_{1–100}$ PFFs used are very homogenous. The binding between α-syn PFFs and LAG3 was examined by incubating α-syn biotinylated PFFs with SH-SY5Y cells transfected with human full-length LAG3, which was further visualized by streptavidin-AP (alkaline phosphatase) staining as described previously (10). The result showed that the pS129 α-syn PFFs exhibited significantly stronger binding with LAG3 in SH-SY5Y cells than that of the WT α-syn PFFs (Fig. 4 *D* and *E* and *SI Appendix*, Fig. S14). In contrast, α-syn$_{1–100}$ PFFs exhibited minimal binding to LAG3 expressed in SH-SY5Y cells. The cellular data are consistent with our biophysical results that the C terminus is vital for the specific binding of α-syn PFFs to LAG3, and S129 phosphorylation significantly promotes the binding.

**α-Syn Fibrils Bind to APLP1 with Similar Electrostatic Interactions.** Amyloid-β precursor-like protein 1 (APLP1) is another receptor found to preferentially bind with α-syn fibrils (10, 15). To understand the mechanism of the α-syn–APLP1 binding, we prepared the recombinant E1 domain of APLP1 (A1E1). We observed the direct binding of A1E1 to α-syn fibrils by TEM using nanogold to indicate the position of the His-tagged A1E1 (Fig. 5*A*). The BLI measurement showed that A1E1 bound to α-syn PFFs with a much higher binding affinity (46.7 ± 0.7 nM) than that bound to the α-syn monomer (0.9 ± 0.2 μM) (Fig. 5*B*).

We next combined NMR spectroscopy, computational modeling, and mutagenesis to characterize the complex structure of A1E1 and α-syn. We built a structure model of A1E1 by homology modeling (*SI Appendix*, Fig. S15) and accomplished the backbone assignment of A1E1 by 3D NMR experiments (*SI Appendix*, Fig. S16). NMR titration studies showed that the addition of substoichiometric α-syn PFFs resulted in a global intensity reduction of the NMR signals (Fig. 5 *C* and *D* and *SI Appendix*, Fig. S17*A*), implying the direct binding between them. While titration with the excess α-syn monomer mainly resulted in CSDs of clustered residues (Fig. 5 *C* and *E* and *SI Appendix*, Fig. S17*B*), which formed a defined, positively charged patch as mapped on the structural model of A1E1 for α-syn binding (Fig. 5*F*). Moreover, titration of A1E1 to the $^{15}$N-α-syn monomer revealed obvious CSDs of the C terminus of α-syn (Fig. 5*G* and *SI Appendix*, Fig. S18), and isolated α-syn$_{101–140}$ binds to A1E1 with an apparent $K_D$ of 2.82 ± 0.06 μM (*SI Appendix*, Fig. S19). In addition, α-syn PFFs alone were digested significantly faster by PK than incubated with A1E1 (*SI Appendix*, Fig. S7). All these results suggest that that same as the interaction to LAG3, the acidic C terminus of α-syn mediates its binding to A1E1.

We further modeled a complex structure of A1E1–α-syn$_{118–140}$ by HADDOCK and MD simulation (*SI Appendix*, Table S1) using the restraints from the NMR data. The structure model showed that A1E1 used the positively charged patch to accommodate the C terminus of α-syn (Fig. 5*H*). Consistent with the NMR and computational results, mutations of either the key positively charged residues (triple mutations of R80E, R82E, and R83E, termed as A1E1_3E) or the C-terminal truncation of α-syn (α-syn$_{1–100}$) completely eliminated the binding of A1E1 to both the α-syn monomer and PFFs (Fig. 5*I*). Same as the interaction of α-syn to L3D1, S129 phosphorylation significantly increased the binding affinity of α-syn PFFs with A1E1 by one order of magnitude, from a $K_D$ value of 46.7 ± 0.7 to 2.0 ± 0.2 nM (Fig. 5 *B* and *I*). Taken together, these results demonstrate that LAG3 and APLP1 bind to α-syn PFFs commonly via electrostatic interactions and highlight the central role of the C terminus of α-syn in mediating the binding of fibrillar forms to different receptors for cell-to-cell transmission.

**The Role of the C Terminus and S129 Phosphorylation of α-Syn PFFs in Neuronal Binding, Internalization, Propagation, and Neurotoxicity.** Since our in vitro study identified that the C terminus and its S129 phosphorylation are vital in the receptor binding of α-syn PFFs, we next sought to examine their roles in primary neurons. Firstly, by performing the cell surface–binding assay with mouse primary cortical neurons, we found that the binding of pS129 PFFs was stronger than that of the WT PFFs, while α-syn$_{1–100}$ PFFs exhibited only minimal binding to neurons (Fig. 6 *A* and *B*). We further measured the endocytosis of α-syn PFFs. WT, pS129, and α-syn$_{1–100}$ PFFs were administered to primary cortical cultures, respectively. The endosomal/lysosomal enrichment fraction was collected by differential centrifugation as published (10). The internalization of WT, pS129, and α-syn$_{1–100}$ PFFs in the enriched endosomal/lysosomal fraction was assessed by immunoblots. The results showed that pS129 α-syn PFFs entered neurons more efficiently than that of the WT α-syn PFFs

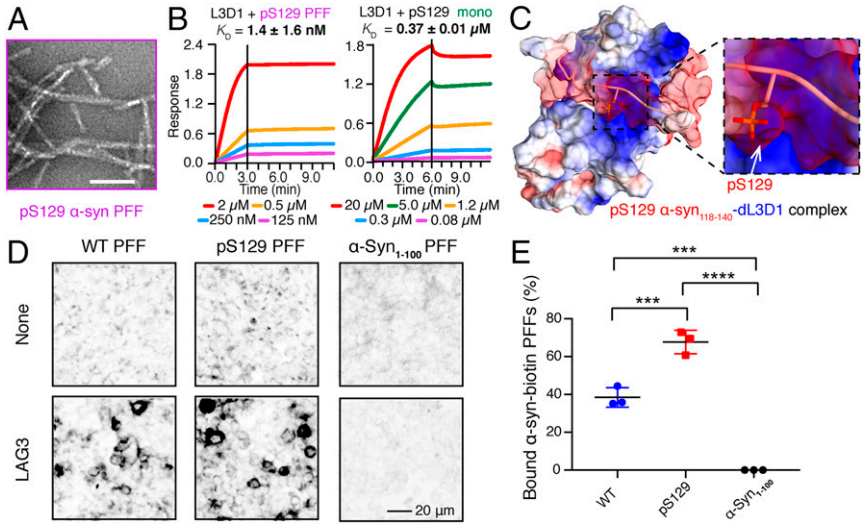


**Fig. 4.** pS129 α-syn fibril exhibits enhanced binding with LAG3 in SH-SY5Y cells. (*A*) The TEM image of pS129 α-syn PFFs. (Scale bar, 200 nm.) (*B*) BLI binding kinetics of L3D1 with pS129 α-syn PFFs (*Left*) and monomers (*Right*). (*C*) The structure model of pS129 α-syn$_{118–140}$-dL3D1 complex built by HADDOCK. pS129 is in contact with the positively charged surface of dL3D1. (*Right*) The binding surface zoomed in. (*D*) High-magnification images of the biotinylated pS129, WT, and α-syn$_{1–100}$ PFFs binding to LAG3-expressing SH-SY5Y cells. (*E*) The statistical analysis is shown. Data are the means ± SEM, $n = 3$ independent experiments. One-way ANOVA followed by Tukey's correction, ***$P < 0.001$, ****$P < 0.0001$.

(Fig. 6*C* and *SI Appendix*, Fig. S20). Of note, most of the α-syn$_{1–100}$ PFFs were barely taken up by neurons (Fig. 6*C* and *SI Appendix*, Fig. S20).

We next characterized the propagation of different α-syn PFFs in primary cultured cortical neurons. A total of 2 wk after the addition of WT, pS129, and α-syn$_{1–100}$ PFFs to primary cortical cultures, we examined immunoblots of α-syn from lysates sequentially extracted in 1% Triton X-100 (TX-soluble), followed by 2% sodium dodecyl sulfate (SDS) (TX-insoluble). The pS129 α-syn PFFs led to more accumulation of α-syn in the TX-insoluble fraction than that of the WT and α-syn$_{1–100}$ PFFs (Fig. 6*D* and *SI Appendix*, Fig. S21). To confirm the role of the C terminus of α-syn in pathology, we added WT or α-syn$_{1–100}$ PFFs to cortical cultures at 7 d and examined the immunoreactivity of anti-pS129 α-syn at 17 d. The α-syn$_{1–100}$ PFFs exhibited only limited propagation as shown by the immunostaining of anti-pS129 compared to the extensive immunoreactivity of WT α-syn PFFs (Fig. 6*E* and *SI Appendix*, Fig. S22).

The treatment of cortical cultures with WT α-syn PFFs led to substantial neuronal cell death as assessed with propidium iodide staining compared with the phosphate-buffered saline (PBS)-treated culture (10, 12) (Fig. 6*F*). The addition of pS129 α-syn PFFs caused significantly more cell death than that of the WT α-syn PFFs, while α-syn$_{1–100}$ PFFs induced only limited neurotoxicity (Fig. 6*F* and *SI Appendix*, Fig. S23). Importantly, LAG3 knockout (LAG3$^{-/-}$) significantly reduced the neurotoxicity caused by WT or pS129 α-syn PFFs (*SI Appendix*, Fig. S24), confirming the important role of LAG3 in this process.

Together, these data show that the C terminus of α-syn is crucial for the binding of exogenous α-syn PFFs to neurons, which can subsequently induce pathological aggregation of endogenous α-syn and neurotoxicity. Furthermore, we show that S129 phosphorylation promotes the internalization of α-syn PFFs via increased binding to neurons, which can then further enhance the propagation and neurotoxicity of α-syn fibrils in the LAG3-dependent manner.

**The Role of S129 Phosphorylation in α-Syn PFF-Induced Neurodegeneration In Vivo.** Since S129 phosphorylation significantly enhances receptor binding, neural propagation, and the toxicity of α-syn PFFs, we finally examined its role in inducing neurodegeneration in vivo. We stereotactically injected WT, α-syn$_{1–100}$, and pS129 α-syn PFFs into the dorsal striatum of α-syn transgenic mice expressing a human α-syn with a familial PD-associated mutation (A53T mice) (36, 37). Between 70 to 80 d after the intrastriatal injection, we performed biochemical and behavioral assays to compare the mice injected with WT, α-syn$_{1–100}$, and pS129 α-syn PFFs. Stereological counting of tyrosine hydroxylase (TH)- and Nissl-positive neurons in the substantia nigra pars compacta (SNpc) revealed a significant loss of dopamine neurons of mice injected with pS129 α-syn PFFs compared to the mice injected with WT, α-syn$_{1–100}$ PFFs, or PBS (Fig. 7 *A–C*). However, there was no significant difference in neuron loss between animals treated with PBS, α-syn$_{1–100}$, and WT PFFs (Fig. 7 *A–C*).

Consistent with the cellular data, intrastriatal injection of pS129 α-syn PFFs exhibited significantly more accumulation of α-syn in the TX-insoluble fraction of the hindbrain region than that of the WT α-syn PFFs (Fig. 7 *D–F*). We further examined the oxidization of α-syn as assessed by immunostaining of anti-Syn505 and found that pS129 α-syn PFFs significantly increased the immunoreactivity of anti-Syn505 in the TX-insoluble fraction of the hindbrain region compared to that of the WT α-syn PFFs (Fig. 7 *D–F*).

The pole test was used to monitor the behavioral consequences of WT, α-syn$_{1–100}$, and pS129 α-syn PFFs injection. There was a marked behavioral impairment induced by WT α-syn PFFs, with increased time to turn and reach the base, compared to that of PBS controls. pS129 α-syn PFFs significantly increased the time on the pole test compared to WT α-syn PFFs, although there was no significant difference between α-syn$_{1–100}$ and WT PFFs or α-syn$_{1–100}$ PFFs and PBS control (Fig. 7*G*). We further performed grip strength testing and found that the injection of WT α-syn PFFs significantly reduced the grip strength of mice compared to that of the PBS control. The pS129 α-syn PFFs–injected mice further reduced grip strength compared to the WT α-syn PFFs–injected mice, while α-syn$_{1–100}$ PFFs–injected mice showed no significant difference with PBS control mice (Fig. 7*H*).

In the open field test, the A53T mice showed hyperactivity at preclinical ages (from 5 mo onward to 5 d before the onset of symptoms) compared to that of WT mice (36, 37). Open field

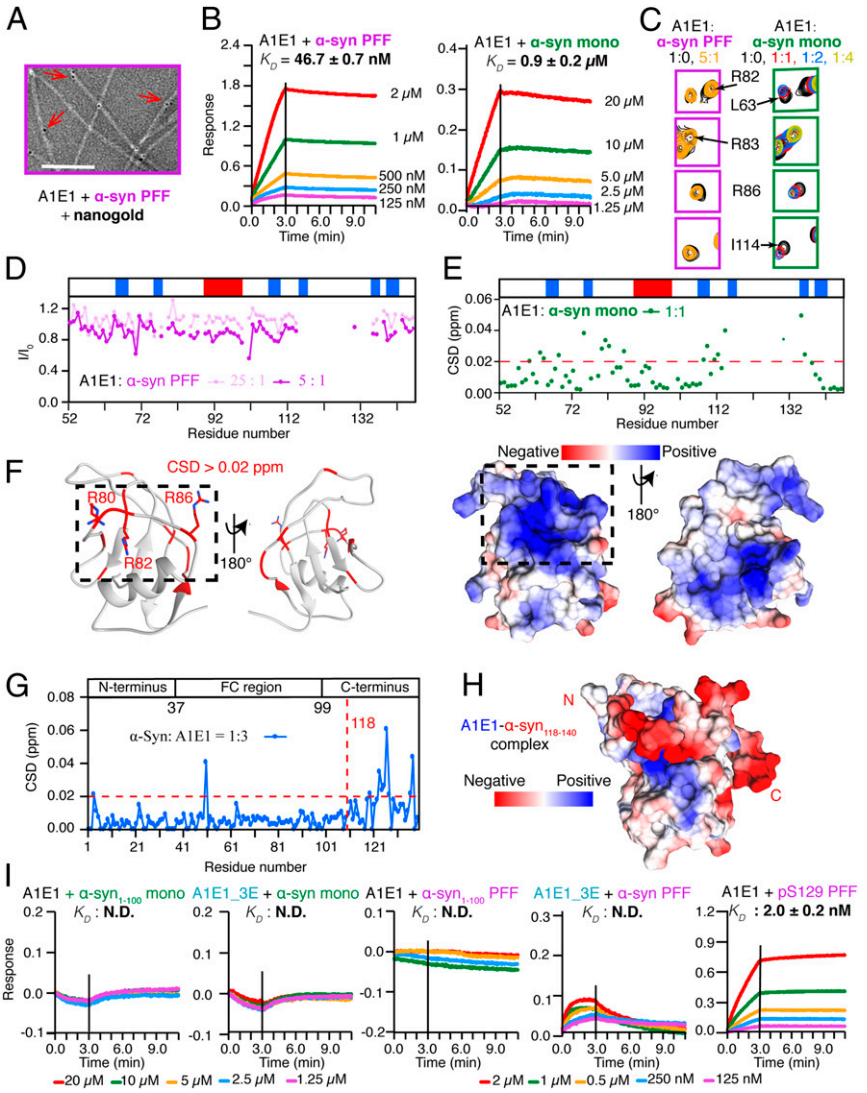


**Fig. 5.** Mechanism of A1E1 binding with α-syn. (*A*) The TEM image of α-syn fibrils incubated with His-tagged A1E1 and nanogolds. The red arrows highlight the attachment of nanogolds on α-syn fibrils via A1E1. (Scale bar, 100 nm.) (*B*) BLI binding kinetics of A1E1 with α-syn PFFs (*Left*) and the α-syn monomer (*Right*). (*C*) Representing resonances from the 2D HSQC spectra of A1E1 upon the titration of α-syn PFFs (*Left*) and the α-syn monomer (*Right*). (*D*) Residue-specific intensity changes ($I/I_0$) of A1E1 in the presence of α-syn PFFs at the indicated concentrations. The secondary structure of A1E1 is shown with a blue bar representing the β strand and a red bar for the α-helix. (*E*) Residue-specific CSDs of A1E1 in the presence of α-syn monomer. The red dashed line highlights the residues with CSD > 0.02 ppm. (*F*) Residues with CSD > 0.02 ppm (red) upon the α-syn monomer titration are mapped on the modeled structure of A1E1 (*Left*). The side chains of key interacting residues of A1E1 including R80, R82, and R86 are shown. Electrostatic surface of A1E1 (*Right*) shows that the interacting surface of A1E1 exhibits a positively charged patch. The dashed boxes highlight the residues of A1E1 with CSDs > 0.02 ppm. (*G*) Calculated CSDs of α-syn in the presence of A1E1 at a molar ratio of 1:3. The red dashed line highlights the residues with CSD > 0.02 ppm. (*H*) Electrostatic surface representation of the structure model of A1E1-α-syn$_{118–140}$ complex, which is built by HADDOCK. The acidic C terminus of α-syn binds to the positively charged patch of A1E1. (*I*) BLI binding kinetics of A1E1 or A1E1_3E with different variants of α-syn monomer and PFFs. N.D., not detectable.

monitoring revealed that injection of pS129 α-syn PFFs significantly increased the activity of A53T mice at 9 to 12 mo of age compared to that of WT α-syn PFFs–injected A53T mice. There was no significant difference in the activity of A53T mice injected with WT, α-syn$_{1–100}$ PFFs, and those injected with PBS (Fig. 7*I*). Altogether, our results demonstrate that S129 phosphorylation of α-syn PFFs leads to exacerbated PD-like neurodegeneration in vivo.

## Discussion

Recent technical advances in cryo-EM have allowed the determination of the atomic structures of pathological fibrils formed by different amyloid proteins including α-syn (20–24), Tau (38–40), and β-amyloid (41). However, we still know very little regarding the spread of the amyloid fibrils in neurodegenerative diseases. In this work, we provide the structural mechanism for the receptor-mediated transmission of α-syn fibrils (Fig. 8). We found that the acidic C terminus of α-syn was the key domain that bound with a positively charged surface on the receptors. The C terminus in monomeric α-syn transiently interacts with the FC region. While under disease conditions, as the FC region self-assembles to drive the formation of amyloid fibrils, the C terminus is released and concentrated on the surface of α-syn fibrils. This conformational rearrangement favors receptor binding and cellular internalization of α-syn. It is worthwhile to note that the receptor binding and cellular uptake of α-syn fibrils are length dependent. It has been reported that short fibrillary samples, especially α-syn with a length of ~50 nm, revealed an enhanced

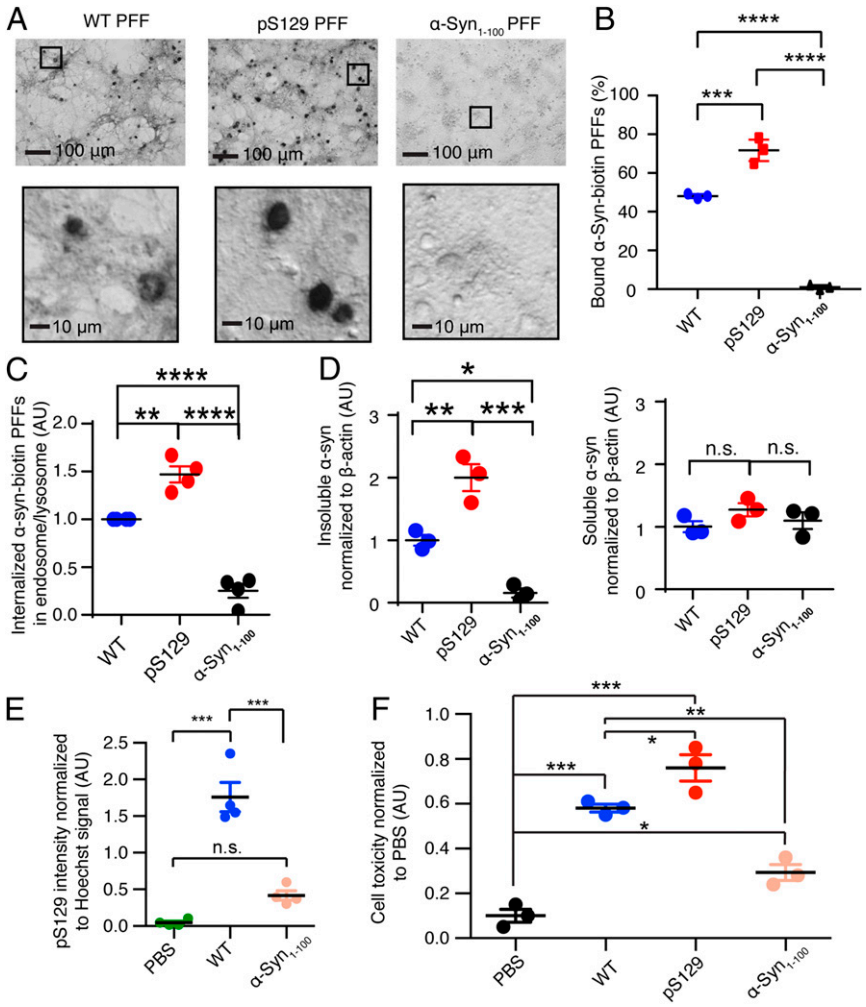


**Fig. 6.** S129 phosphorylation and C terminus are crucial for internalization, propagation, and neurotoxicity of α-syn PFFs in primary cultured cortical neurons. (*A*) Low (*Top*) and high (*Bottom*) magnification views of images of pS129, WT, and α-syn$_{1-100}$ PFFs binding to neurons (14 d in vitro). The binding signal is assessed by means of an alkaline phosphatase assay. (*B*) Quantification of *A* by Scatchard analysis. Data are the means ± SEM, $n = 3$ independent experiments. One-way ANOVA followed by Tukey's correction, ***$P < 0.001$, ****$P < 0.0001$. (*C*) Quantification of the immunoblots analysis of the enriched endosomal/lysosomal fraction confirms that biotin-labeled pS129 α-syn PFFs enter mouse primary cortical neurons more efficiently than that of the WT and α-syn$_{1-100}$ PFFs. Data are the means ± SEM, $n = 3$. Student's *t* test. (*D*) Quantification of immunoblots in WT neuron lysates for insoluble (*Left*) and soluble (*Right*) α-syn. pS129 α-syn PFFs can induce more insoluble α-syn aggregates than that of the WT and α-syn$_{1-100}$ PFFs. The results are shown as means ± SEM. One-way ANOVA followed by Tukey's correction. No significant difference is shown in soluble fraction. (*E*) Quantification of α-syn pathology induced by WT and α-syn$_{1-100}$ PFFs to mouse primary cortical neurons, which was assessed with anti-pS129 immunostaining 10 d after α-syn PFF treatment. WT α-syn PFFs can induce substantial immunoreactivity of anti-pS129, whereas C terminus truncation (α-syn$_{1-100}$ PFFs) reduces the pS129 pathology significantly. (*F*) Quantification of the toxicity of WT, pS129, and α-syn$_{1-100}$ PFFs to mouse primary cortical neurons. pS129 α-syn PFFs exhibit more toxicity than that of WT PFFs, and α-syn$_{1-100}$ PFFs exhibit much less neurotoxicity than WT PFFs. Data in (*E* and *F*) are the means ± SEM, $n = 3$, one-way ANOVA followed by Tukey's correction, *$P < 0.05$, **$P < 0.01$, ***$P < 0.001$.

accumulation of phosphorylated α-syn than their longer counterparts (42, 43). We also found that α-syn PFFs with a longer length (100 to 200 nm) were much weaker than those with a shorter length (~50 nm) in both L3D1 binding and attachment to primary cortical neurons (*SI Appendix*, Fig. S25). This length-dependent phenomenon quite makes sense based on the binding mechanism shown in this work. Fibril formation on one hand exposes and condenses the C terminus for receptor binding, while on the other hand limits the mobility of α-syn molecules. Given that the receptors are fixed on the membrane surface, long fibrils may therefore oversaturate the receptor binding. Another note is that we only used isolated domains of the receptors for the in vitro experiments in this study. We show here that isolated D1 of LAG3 binds strongly to α-syn PFFs, which is consistent with our previous work showing that D1 is essential for the binding of receptors to α-syn PFFs (10). However, it is likely that the other domains of the receptors may also play a role in the binding.

Phosphorylation at S129 is a characteristic modification of pathological α-syn that accumulates in Lewy bodies and Lewy neurites (25, 26, 44). However, whether this phosphorylation inhibits or facilitates α-syn aggregation and neurotoxicity remains controversial (45–49). This has hindered the drug development targeting the kinases or phosphatases regulating this phosphorylation. Our work demonstrates that S129 phosphorylation dramatically promotes the binding of α-syn fibrils to its receptors (LAG3 and APLP1) by strengthening the electrostatic interaction (Fig. 8). This leads to exacerbation of pathological α-syn fibrils transmission and neurodegeneration.

The C-terminal truncation of α-syn has been found in familial PD and animal models (50, 51). Previous studies showed that the C

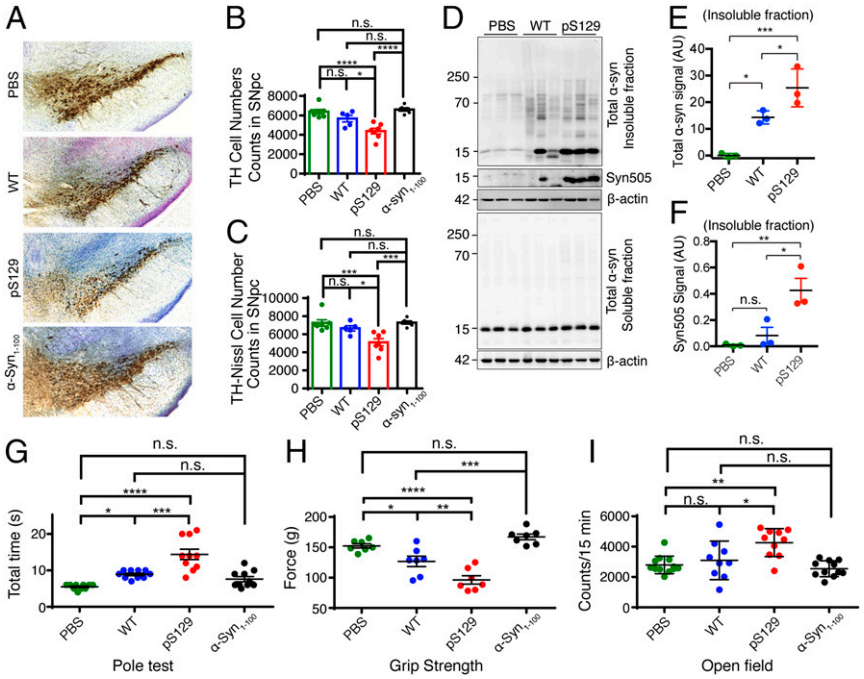


**Fig. 7.** S129 phosphorylation in α-syn PFF-induced neurodegeneration in vivo. (*A*) Representative TH (tyrosine hydroxylase) immunohistochemistry and Nissl staining images of dopamine neurons in the SNpc of WT, α-syn$_{1–100}$, and pS129 PFF-injected hemisphere in the hA53T mice. (*B* and *C*) Stereological counting of the number of TH- and Nissl-positive neurons in the SNpc via unbiased stereological analysis after 2 to 3 mo of α-syn PFF injection in the hA53T mice (PBS: $n = 7$; WT α-syn PFFs: $n = 5$; pS129 α-syn PFFs: $n = 7$, α-syn$_{1–100}$ PFFs: $n = 5$). Data are the means ± SEM, one-way ANOVA with Tukey's correction; $^*P < 0.05$, $^{**}P < 0.01$, $^{***}P < 0.001$, $^{****}P < 0.0001$, n.s., not significant. (*D–F*) Immunoblots of the hindbrain lysates of hA53T mice 3 mo after intrastriatal injection of WT PFFs, pS129 α-syn PFFs, and PBS. pS129 α-syn PFF injection exhibits significantly increased signals of insoluble α-syn and oxidative α-syn in the hindbrain compared to that of WT PFFs. Data are the means ± SEM, $n = 3$ individual experiments, one-way ANOVA with Tukey's correction. $^*P < 0.05$, $^{**}P < 0.01$, n.s., not significant. (*G–I*) Behavioral abnormalities of PBS-, WT PFFs-, α-syn$_{1–100}$ PFFs-, and pS129 α-syn PFFs injected hA53T mice at 2 mo measured by the pole test (*G*, $n = 8$ mice per group), the grip strength test (*H*, $n = 7$ mice per group), and the open field (*I*, $n = 9$ to 12 mice). Data are the means ± SEM, one-way ANOVA with Tukey's correction. $^*P < 0.05$, $^{**}P < 0.01$, $^{***}P < 0.001$, $^{****}P < 0.0001$, n.s., not significant.

terminus of α-syn is cleaved by cathepsin in the endosome–lysosome pathway (52) following the internalization of the exogenous α-syn fibrils. Other mechanisms may also involve in the cleavage of the C terminus (53). Intriguingly, the C-terminal truncation exhibits enhanced capability for self-assembly and lateral association as well as seeding full-length α-syn to form pathological fibrils (48, 54, 55). However, the C-terminal–truncated α-syn PFFs alone exhibit a severely impaired capability for inducing the aggregation of endogenous WT α-syn in primary neurons (56). Together with these findings, our work indicates that different variants/modifications of α-syn may influence the spread of α-syn pathology at different stages. A possible simplified scenario for the cell-to-cell transmission of α-syn fibrils might be that α-syn forms amyloid fibrils at the primary foci. Exocytosis releases the pathological fibrils that subsequently bind with the receptors and enter the next neurons by endocytosis. The exogenous pathological fibrils might encounter digestion and degradation at the new foci and lose their C termini, while the truncated fibrils are still (if not more) able to seed the endogenous α-syn to propagate the pathological aggregation (Fig. 8).

Despite that the primary pathogenesis of PD can be attributed to various causes, subsequent progression may undergo a common process featuring the spread of α-syn fibrils (3, 7, 11). We found that receptors LAG3 and APLP1 share a common positive patch on the domain surface to bind the C terminus of α-syn fibrils. Thus, to block α-syn transmission, targeting on the interaction between the C terminus of α-syn and the positive surface of the receptors is a promising strategy to treat PD and other α-synucleinopathies. Several other receptors have recently been identified to bind different species of α-syn (57–59). Thus, further studies will be required to explore whether they employ a similar mechanism for α-syn binding. Furthermore, we notice that the binding surface of LAG3 for α-syn fibrils is distinct from that for MHC-II (28). The latter is important for the normal function of LAG3 in the immune response (28). This finding further encourages the targeting on the binding of α-syn and the receptors. Peptide mimics, antibodies, and small compounds that compete with this binding might be promising drug candidates to contribute to block the spread of α-syn fibrils and arrest PD progression. At the same time, it must be noted that receptor-mediated transmission is just one side of the spread of α-syn fibrils. Much is still to be learned in aim to effectively block the cell-to-cell transmission of α-syn fibrils.

## Materials and Methods

**BLI.** The binding kinetics were measured on an ForteBio Octet RED96 system (Pall ForteBio LLC). Standard BLI protocol was performed except that an auto-inhibition step was used to eliminate the nonspecifically binding of α-syn monomer/PFFs to biosensors. The resulting curves were corrected using the blank reference and analyzed by the ForteBio Data Analysis software 9.0.

**NMR Spectroscopy.** All NMR experiments were collected at 298 K in the NMR buffer of 25 mM $Na_2HPO_4$, 50 mM NaCl, and 10% (vol/vol) $D_2O$ at pH 7.0. HNCACB and CBCA(CO)NH experiments were performed to obtain the chemical shift assignment of backbone atoms of dL3D1 and A1E1. 2D HSQC were collected on a Bruker 900 MHz spectrometer equipped with a cryogenic probe. PRE effects were measured from the peak intensity ratios from the HSQC spectra of $^{15}$N-MTSL-A124C/E35C α-syn without/with 1 mM sodium ascorbate.

**Structural Modeling of L3D1 and A1E1.** The homology modeling of L3D1/A1E1 was performed using the Iterative Threading ASSEmbly Refinement (I-TASSER) server and Rosetta software package following standard protocols.

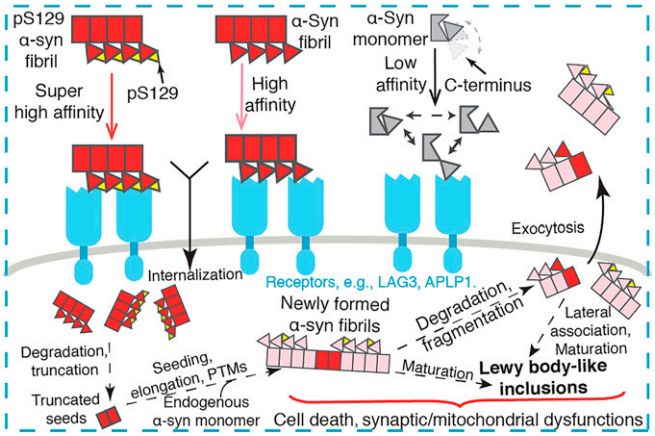


**Fig. 8.** Schematic diagram of α-syn pathological transmission. Over the progression of PD and α-synucleinopathies, α-syn aggregation spreads from cell to cell in the brain. α-Syn monomer, fibril, and pS129 fibril exhibit distinct binding affinities to the receptors (e.g., LAG3 and APLP1) depending on the structural arrangement and chemical property of the C terminus of α-syn; thus, they show different efficiency in the spread of α-syn pathology. The internalized α-syn fibrils may undergo degradation and truncation of the C terminus while maintaining the high ability of seeding the formation of new fibrils in the transfected neurons.

**HADDOCK and MD Simulation.** The structural coordinates of dL3D1 were from our modeled structure of L3D1 by eliminating the extra loop residues (residues 74 to 92). The structural coordinates of $\alpha\text{-syn}_{118-140}$ were extracted from the full-length α-syn structures with Protein Data Bank codes of 1xq8 (one conformation), 2kkw (one conformation), and 2n0a (10 conformations); a total of 12 truncated structures. The docking and refinement studies were carried out using the standard HADDOCK protocol with a number of ambiguous interaction restraints and the interface residues that were identified from NMR titrations.

The MD simulations of the complex were performed using Amber 14 and Amber 16 with the GPU accelerated version of PMEMD using standard protocols. The MD trajectories were postprocessed to compute free energies of binding using the MMPBSA.py program, and the energy decomposition per residue was performed from MM-GBSA calculations.

**Immunoblot of WT, pS129, and $\alpha\text{-Syn}_{1-100}$ PFFs.** PFFs samples were separated on SDS-polyacrylamide gels (12%) and transferred to nitrocellulose membranes. The membranes were blocked in 5% bovine serum albumin in Tris-buffered saline Tween 20 and then incubated with primary antibody for α-syn (BD Transduction Laboratories, 610787) or streptavidin-HRP (CST 3999S). Target antigens were developed by Chemiluminescent Substrate (SuperSignal West Pico PLUS, Thermo, 34578) and imaged by ImageQuant LAS 4000 mini scanner (GE Healthcare Life Sciences).

**Primary Neuronal Cultures, PFFs Transduction for Pathology and Neurotoxicity.** α-Syn PFFs were added at 7 d in vitro (5 μg/mL) primary neuronal cultures. For pathology experiments, primary cultures were fixed with 4% paraformaldehyde 7 to 10 d after PFF treatment followed by immunostaining of anti-phosphorylated S129 α-syn antibody (EP1536Y, ab51253). In a neurotoxicity assay, primary cultures were washed with prewarmed Neurobasal medium and then treated with 2.5 μM propidium iodide and 7 μM Hoechst 33342. Neurotoxicity was also measured by immunostaining of anti-NeuN antibody (A60, MAB377, EMD Millipore) in 4% paraformaldehyde-fixed primary cultures.

**Cell Surface–Binding Assays.** The cell surface–binding assay was performed at room temperature (~25 °C) and followed the established protocol (10).

**Endosome/Lysosome Enrichment.** The experiments performed followed the previous publication (10). The samples were transferred to nitrocellulose membranes and incubated with the primary antibody for α-syn (BD Transduction Laboratories, 610787) followed by incubation with secondary antibody. Target antigens were developed by Chemiluminescent Substrate (SuperSignal West Femto Maximum Sensitivity, Thermo, 34095).

**Primary Neuronal and Brain Tissue Lysates for Insoluble α-Syn.** Primary neuronal cultures were collected 12 to 15 d after α-syn PFF treatment. Brain tissues were collected from perfused mice with ice-cold PBS 2.5 mo after α-syn PFF injection. The cultures or tissues were homogenized with lysis buffer (50 mM Tris, 150 mM NaCl, and 1% Triton X-100) containing protease and phosphatase inhibitor mixture (Millipore Sigma). Cell lysates were centrifuged at 20,000 *g* for 20 min, and the supernatants were collected as soluble fraction. The pellets were washed three times and resuspended with lysis buffer containing 2% SDS. Then, the samples were sonicated and centrifuged at 18,000 *g* for 20 min. The supernatants were collected as insoluble fraction.

**Grip Strength Test, Pole Test, and Open Field Test.** All test experiments were performed 2 mo after α-syn PFF stereotaxic injection as previously described (10).

More details about the methods are given in *SI Appendix, Detailed Materials and Methods*.

**Data Availability.** Chemical shift assignments for dL3D1 and A1E1 have been deposited in the Biological Magnetic Resonance Bank with the identification numbers of 50035 and 50034, respectively. All data and procedures are provided in the manuscript and *SI Appendix*.

**ACKNOWLEDGMENTS.** We thank staff members of the National Facility for Protein Science in Shanghai, Zhangjiang Laboratory, China for providing technical support and assistance in NMR and BLI data collection. This work was supported by the National Natural Science Foundation of China (Grant No. 91853113 to C.L. and 92053108 to Y.-M.L.), the National Key R&D Program of China (Grant No. 2019YFE0120600 to C.L., 2018YFA0507600 and 2019YFA0904200 to Y.-M.L.), the Science and Technology Commission of Shanghai Municipality (Grant No. 18JC1420500 to C.L.), the Shanghai Municipal Science and Technology Major Project (Grant No. 2019SHZDZX02 to C.L.), and the Shanghai Science and Technology Committee (Grant No. 20XD1425000 to C.L.). The "Eastern Scholar" project was supported by the Shanghai Municipal Education Commission to D.L. X.M. was supported by R01 NS107318, K01 AG056841, the Parkinson's Foundation Stanley Fahn Junior Faculty Award PF-JFA-1933, and Maryland Stem Cell Research Foundation Discovery Award 2019-MSCRFD-4292 from the American Parkinson's Disease Association. This work was supported by the JPB Foundation.

1. R. Riek, D. S. Eisenberg, The activities of amyloids from a structural perspective. *Nature* **539**, 227–235 (2016).
2. C. M. Dobson, T. P. J. Knowles, M. Vendruscolo, The amyloid phenomenon and its significance in biology and medicine. *Cold Spring Harb. Perspect. Biol.* **12**, a033878 (2019).
3. S. Kim *et al.*, Transneuronal propagation of pathologic alpha-synuclein from the gut to the brain models Parkinson's disease. *Neuron* **103**, 627–641.e7 (2019).
4. J. H. Kordower, Y. Chu, R. A. Hauser, T. B. Freeman, C. W. Olanow, Lewy body-like pathology in long-term embryonic nigral transplants in Parkinson's disease. *Nat. Med.* **14**, 504–506 (2008).
5. H. Braak, D. Sandmann-Keil, W. Gai, E. Braak, Extensive axonal Lewy neurites in Parkinson's disease: A novel pathological feature revealed by alpha-synuclein immunocytochemistry. *Neurosci. Lett.* **265**, 67–69 (1999).
6. H. Braak, R. A. de Vos, J. Bohl, K. Del Tredici, Gastric alpha-synuclein immunoreactive inclusions in Meissner's and Auerbach's plexuses in cases staged for Parkinson's disease-related brain pathology. *Neurosci. Lett.* **396**, 67–72 (2006).
7. H. Braak *et al.*, Staging of brain pathology related to sporadic Parkinson's disease. *Neurobiol. Aging* **24**, 197–211 (2003).
8. J. Y. Li *et al.*, Lewy bodies in grafted neurons in subjects with Parkinson's disease suggest host-to-graft disease propagation. *Nat. Med.* **14**, 501–503 (2008).
9. S. B. Prusiner *et al.*, Evidence for α-synuclein prions causing multiple system atrophy in humans with parkinsonism. *Proc. Natl. Acad. Sci. U.S.A.* **112**, E5308–E5317 (2015).
10. X. Mao *et al.*, Pathological α-synuclein transmission initiated by binding lymphocyte-activation gene 3. *Science* **353**, aah3374 (2016).
11. K. C. Luk *et al.*, Pathological α-synuclein transmission initiates Parkinson-like neurodegeneration in nontransgenic mice. *Science* **338**, 949–953 (2012).
12. T. I. Kam *et al.*, Poly(ADP-ribose) drives pathologic α-synuclein neurodegeneration in Parkinson's disease. *Science* **362**, eaat8407 (2018).
13. K. C. Luk *et al.*, Intracerebral inoculation of pathological α-synuclein initiates a rapidly progressive neurodegenerative α-synucleinopathy in mice. *J. Exp. Med.* **209**, 975–986 (2012).
14. H. Gu *et al.*, Lymphocyte activation gene 3 (Lag3) contributes to α-synucleinopathy in α-synuclein transgenic mice. *Front. Cell. Neurosci.* **15**, 656426 (2021).
15. X. Mao *et al.*, Aplp1 and the Aplp1-Lag3 Complex facilitates transmission of pathologic α-synuclein. bioRxiv [Preprint] (2021). https://doi.org/10.1101/2021.05.01.442157 (Accessed 1 May 2021).
16. F. X. Theillet *et al.*, Structural disorder of monomeric α-synuclein persists in mammalian cells. *Nature* **530**, 45–50 (2016).
17. J. Diao *et al.*, Native α-synuclein induces clustering of synaptic-vesicle mimics via binding to phospholipids and synaptobrevin-2/VAMP2. *eLife* **2**, e00592 (2013).
18. J. Burré *et al.*, Alpha-synuclein promotes SNARE-complex assembly in vivo and in vitro. *Science* **329**, 1663–1667 (2010).

19. C. C. Jao, B. G. Hegde, J. Chen, I. S. Haworth, R. Langen, Structure of membrane-bound alpha-synuclein from site-directed spin labeling and computational refinement. *Proc. Natl. Acad. Sci. U.S.A.* **105**, 19666–19671 (2008).
20. Y. Li *et al*., Amyloid fibril structure of α-synuclein determined by cryo-electron microscopy. *Cell Res.* **28**, 897–903 (2018).
21. B. Li *et al*., Cryo-EM of full-length α-synuclein reveals fibril polymorphs with a common structural kernel. *Nat. Commun.* **9**, 3609 (2018).
22. R. Guerrero-Ferreira *et al*., Cryo-EM structure of alpha-synuclein fibrils. *eLife* **7**, 3609 (2018).
23. M. Schweighauser *et al*., Structures of α-synuclein filaments from multiple system atrophy. *Nature* **585**, 464–469 (2020).
24. Y. Sun *et al*., Cryo-EM structure of full-length α-synuclein amyloid fibril with Parkinson's disease familial A53T mutation. *Cell Res.* **30**, 360–362 (2020).
25. J. P. Anderson *et al*., Phosphorylation of Ser-129 is the dominant pathological modification of alpha-synuclein in familial and sporadic Lewy body disease. *J. Biol. Chem.* **281**, 29739–29752 (2006).
26. H. Fujiwara *et al*., alpha-Synuclein is phosphorylated in synucleinopathy lesions. *Nat. Cell Biol.* **4**, 160–164 (2002).
27. A. W. Schmid, B. Fauvet, M. Moniatte, H. A. Lashuel, Alpha-synuclein post-translational modifications as potential biomarkers for Parkinson disease and other synucleinopathies. *Mol. Cell. Proteomics* **12**, 3543–3558 (2013).
28. B. Huard *et al*., Characterization of the major histocompatibility complex class II binding site on LAG-3 protein. *Proc. Natl. Acad. Sci. U.S.A.* **94**, 5744–5749 (1997).
29. G. C. P. van Zundert *et al*., The HADDOCK2.2 web server: User-friendly integrative modeling of biomolecular complexes. *J. Mol. Biol.* **428**, 720–725 (2016).
30. M. M. Dedmon, K. Lindorff-Larsen, J. Christodoulou, M. Vendruscolo, C. M. Dobson, Mapping long-range interactions in alpha-synuclein using spin-label NMR and ensemble molecular dynamics simulations. *J. Am. Chem. Soc.* **127**, 476–477 (2005).
31. C. W. Bertoncini *et al*., Release of long-range tertiary interactions potentiates aggregation of natively unstructured alpha-synuclein. *Proc. Natl. Acad. Sci. U.S.A.* **102**, 1430–1435 (2005).
32. C. P. A. Doherty *et al*., A short motif in the N-terminal region of α-synuclein is critical for both aggregation and function. *Nat. Struct. Mol. Biol.* **27**, 249–259 (2020).
33. M. Hejjaoui *et al*., Elucidating the role of C-terminal post-translational modifications using protein semisynthesis strategies: α-synuclein phosphorylation at tyrosine 125. *J. Am. Chem. Soc.* **134**, 5196–5210 (2012).
34. B. Fauvet, H. A. Lashuel, Semisynthesis and enzymatic preparation of post-translationally modified alpha-synuclein. *Methods Mol. Biol.* **1345**, 3–20 (2016).
35. J. D. Graef *et al*., Characterization of pathology-inducing α-synuclein species from human diseased brain tissue. bioRxiv [Preprint] (2019). https://doi.org/10.1101/588335 (Accessed 25 March 2019).
36. S. Brahmachari *et al*., Activation of tyrosine kinase c-Abl contributes to α-synuclein-induced neurodegeneration. *J. Clin. Invest.* **126**, 2970–2988 (2016).
37. M. K. Lee *et al*., Human alpha-synuclein-harboring familial Parkinson's disease-linked Ala-53--> Thr mutation causes neurodegenerative disease with alpha-synuclein aggregation in transgenic mice. *Proc. Natl. Acad. Sci. U.S.A.* **99**, 8968–8973 (2002).
38. B. Falcon *et al*., Novel tau filament fold in chronic traumatic encephalopathy encloses hydrophobic molecules. *Nature* **568**, 420–423 (2019).
39. B. Falcon *et al*., Structures of filaments from Pick's disease reveal a novel tau protein fold. *Nature* **561**, 137–140 (2018).
40. A. W. P. Fitzpatrick *et al*., Cryo-EM structures of tau filaments from Alzheimer's disease. *Nature* **547**, 185–190 (2017).
41. L. Gremer *et al*., Fibril structure of amyloid-β(1-42) by cryo-electron microscopy. *Science* **358**, 116–119 (2017).
42. W. F. Xue *et al*., Fibril fragmentation enhances amyloid cytotoxicity. *J. Biol. Chem.* **284**, 34272–34282 (2009).
43. A. Tarutani *et al*., The effect of fragmented pathogenic α-synuclein seeds on prion-like propagation. *J. Biol. Chem.* **291**, 18675–18688 (2016).
44. M. E. Moors *et al*., The orchestration of subcellular alpha-synuclein pathology in the Parkinson's disease brain revealed by STED microscopy. bioRxiv [Preprint] (2019). https://doi.org/10.1101/470476 (Accessed 17 September 2019).
45. M. R. Ma, Z. W. Hu, Y. F. Zhao, Y. X. Chen, Y. M. Li, Phosphorylation induces distinct alpha-synuclein strain formation. *Sci. Rep.* **6**, 37130 (2016).
46. K. E. Paleologou *et al*., Phosphorylation at Ser-129 but not the phosphomimics S129E/D inhibits the fibrillation of alpha-synuclein. *J. Biol. Chem.* **283**, 16895–16905 (2008).
47. O. S. Gorbatyuk *et al*., The phosphorylation state of Ser-129 in human alpha-synuclein determines neurodegeneration in a rat model of Parkinson disease. *Proc. Natl. Acad. Sci. U.S.A.* **105**, 763–768 (2008).
48. A. L. Mahul-Mellier *et al*., The process of Lewy body formation, rather than simply α-synuclein fibrillization, is one of the major drivers of neurodegeneration. *Proc. Natl. Acad. Sci. U.S.A.* **117**, 4971–4982 (2020).
49. A.-L. Mahul-Mellier *et al*., The making of a Lewy body: The role of α-synuclein post-fibrillization modifications in regulating the formation and the maturation of pathological inclusions. bioRxiv [Preprint] (2018). https://doi.org/10.1101/500058 (Accessed 19 December 2018).
50. G. Muntané, I. Ferrer, M. Martinez-Vicente, α-synuclein phosphorylation and truncation are normal events in the adult human brain. *Neuroscience* **200**, 106–119 (2012).
51. W. Li *et al*., Aggregation promoting C-terminal truncation of alpha-synuclein is a normal cellular process and is enhanced by the familial Parkinson's disease-linked mutations. *Proc. Natl. Acad. Sci. U.S.A.* **102**, 2162–2167 (2005).
52. R. P. McGlinchey *et al*., C-terminal α-synuclein truncations are linked to cysteine cathepsin activity in Parkinson's disease. *J. Biol. Chem.* **294**, 9973–9984 (2019).
53. M. Karampetsou *et al*., Phosphorylated exogenous alpha-synuclein fibrils exacerbate pathology and induce neuronal dysfunction in mice. *Sci. Rep.* **7**, 16533 (2017).
54. A. Oueslati, M. Fournier, H. A. Lashuel, Role of post-translational modifications in modulating the structure, function and toxicity of alpha-synuclein: Implications for Parkinson's disease pathogenesis and therapies. *Prog. Brain Res.* **183**, 115–145 (2010).
55. Z. A. Sorrentino *et al*., Physiological C-terminal truncation of α-synuclein potentiates the prion-like formation of pathological inclusions. *J. Biol. Chem.* **293**, 18914–18932 (2018).
56. K. C. Luk *et al*., Molecular and biological compatibility with host alpha-synuclein influences fibril pathogenicity. *Cell Rep.* **16**, 3373–3387 (2016).
57. Y. R. Choi *et al*., Prion-like propagation of α-Synuclein is regulated by the FcγRIIB-SHP-1/2 signaling pathway in neurons. *Cell Rep.* **22**, 136–148 (2018).
58. M. Birol, S. P. Wojcik, A. D. Miranker, E. Rhoades, Identification of N-linked glycans as specific mediators of neuronal uptake of acetylated α-Synuclein. *PLoS Biol.* **17**, e3000318 (2019).
59. C. Kim *et al*., Neuron-released oligomeric α-synuclein is an endogenous agonist of TLR2 for paracrine activation of microglia. *Nat. Commun.* **4**, 1562 (2013).